Polyoxometalates

RESEARCH ARTICLE

Sulfate-guided assembly of a fully closed {Mo192} molybdenum blue capsule with accessible Mo sites for selective phenol oxidation

Jialiang Sun, Huili Fan, Haojie Xu, Pengtao Ma, Chao Zhang ✉, Jingping Wang ✉ and Jingyang Niu ✉

Henan Key Laboratory of Polyoxometalate Chemistry, College of Chemistry and Molecular Sciences, Henan University, Kaifeng 475004, China

Received: 23 July 2026; **Revised:** 27 August 2026; **Accepted:** 1 September 2026

✉ Address correspondence to Chao Zhang, zhangchao@henu.edu.cn; Jingping Wang, jpwang@henu.edu.cn; Jingyang Niu, jyniu@henu.edu.cn

Cite This: *Polyoxometalates*, 2027, *6*, 9140158

Read Online

ABSTRACT: Fully closed molybdenum blue cages remain difficult to prepare because long-range shell closure needs to be balanced with the stability of a mixed-valence Mo^{VI}/Mo^{V} framework. Retaining accessible surface metal sites adds a further challenge when such cages are considered for catalysis. Here we report a sulfate-guided fragment/anion co-assembly strategy for the synthesis of a capsule-shaped {Mo192} molybdenum blue cage, formulated as $K_6Na_{20}[H_{44}Mo^{VI}_{130}Mo^{V}_{62}O_{548}(H_2O)_{102}(OH)_{44}(SO_4)_{10}]\cdot 238H_2O$. The cluster is obtained from a Waugh-type $K_6MnMo_9O_{32}\cdot 6H_2O$ precursor and molybdate under acidic, reducing, and hydrothermal conditions. Single-crystal X-ray diffraction reveals two fused {Mo96} half-shells, inward sulfate-bound {S-Mo6} units, equatorial {Mo2}-based connections, and continuous windows. The inward-facing sulfate ligands help support shell curvature without blocking the outer surface of the cage. Redox titration, bond-valence-sum analysis, and XPS indicate a mixed Mo^{VI}/Mo^{V} framework with an overall reduction degree of ca. 32%. The accessible mixed-valence cage was further evaluated in the tert-butyl hydroperoxide (TBHP) oxidation of 2-tert-butylphenol, giving 99% conversion and 99% selectivity for 2-tert-butyl-*p*-benzoquinone at 70 °C in 6 h. Hot-filtration, ICP-OES, recycling, FT-IR, and PXRD results support {Mo192} as the major recoverable catalytic phase. These results suggest that internal anion support is a useful way to assist the closure of giant POM cages while retaining surface accessibility for catalytic function.

KEYWORDS: polyoxometalate; molybdenum blue; mixed-valence cluster; hindered phenol oxidation.

1 Introduction

Polyoxometalates (POMs) are discrete metal–oxide clusters with well-defined structures and rich redox chemistry [1–3]. Their structural diversity and reversible redox behaviour make them useful in catalysis, energy conversion, and functional materials [4–7]. Recent studies further illustrate that the structural and electronic tunability of POM-based systems can influence charge transfer, catalytic-site environments, and product-selective organic transformations, including in photocatalytic systems [8–10]. More broadly, recent studies have shown that structurally modulated POM building blocks can direct the assembly of high-nuclearity metal clusters and regulate their topology, intercluster organization, metal-site environments, and functional properties [11–13]. These studies illustrate the broader potential of POM-based structural design for controlling cluster architecture and site accessibility. Among them, high-nuclearity molybdenum blue (MB) clusters occupy a special position [14–17]. They illustrate how multiple Mo–O units can assemble into large mixed-valence architectures under controlled reduction, acidity, and temperature conditions. Rings, shells, and cage-like MB clusters have been reported, and these structures have provided useful models for understanding the growth of giant molecular oxides [18–25].

Fully closed MB cages are much less common than open rings or partially closed shells [26–33]. Their formation requires the shell to close over a long range while the reduced Mo^{VI}/Mo^{V} framework remains stable. These two requirements are not easy to satisfy at the same time. Open rings can release strain through unclosed edges, but closed cages must maintain curvature throughout the whole framework. The process is also sensitive to reduced Mo^{V} centres, protonated oxygen sites, counter cations, and internal anions [3,21,22,34,35]. Known closed or near-closed examples, including K-{Mo132}, L-{Mo132}, {Mo260}, and recently reported compressed MB ellipsoids, show that such architectures are accessible [26–29,36]. Even so, controlled access to larger fully closed MB cages remains limited.

A further challenge appears when closed MB cages are considered as functional materials. Well-defined internal cavities and shell windows in POM architectures can influence mass/ion transport and broader structure–function relationships [37]. Previous studies on porous {Mo132}-type molecular capsules have shown that their pore openings can regulate the uptake, release, and exchange of guest molecules and ligands [38,39]. These capsules can also provide

chemically active confined environments. For example, catalytic cleavage of methyl tert-butyl ether was attributed to hydrated {Mo2^{V}} linker sites inside the capsule, whose accessibility was regulated by internally bound acetate ligands and flexible pore openings [38]. Related computational and experimental studies showed that internal Mo sites and confined water molecules can participate in the catalytic hydration of CO_2 [40]. These studies demonstrate that the cavity and pore system of a molecular POM capsule can contribute to its function rather than serving solely as a structural void.

A closed cage must have sufficient internal support to maintain its curvature, while a functional catalyst must also retain accessible sites for reaction components. If internal ligands or linkers interfere with access to the outer surface, the functional utility of the cage may be diminished. Sulfate and sulfite ligands are often found in MB structures, where they are associated with curved local motifs and contribute to shell stabilization [14,17,19,20,36]. These observations suggest that anion-assisted assembly may provide a useful approach to constructing closed cages. An important structural objective is therefore to orient the supporting anions toward the inner cavity while preserving access to the external Mo–O surface.

Selective oxidation of hindered phenols provides a useful functional test for this type of structure [6,41–44]. Alkyl-substituted *p*-benzoquinones are valuable intermediates in fine chemicals and materials chemistry. Heterogeneous oxidation strategies for benzoquinone synthesis from phenolic and lignin-derived substrates have also been explored [45]. However, direct oxidation of hindered phenols remains challenging [6,41,42,46–48]. Bulky substituents can limit access to catalytic sites. Overoxidation and oxidative coupling can reduce product selectivity. A suitable molecular oxide catalyst should therefore combine accessible redox-active sites with structural stability under oxidative conditions. For a closed MB cage, this reaction tests whether shell closure can be achieved without sacrificing surface accessibility.

Here we report a sulfate-guided fragment/anion co-assembly route to a fully closed capsule-shaped {Mo192} molybdenum blue cage. Waugh-type $K_6MnMo_9O_{32}\cdot 6H_2O$ ({$MnMo_9$}) is used as a preorganized Mo–O precursor [49]. H_2SO_4 provides both the acidic medium and sulfate anions. Under acidic, reducing, and hydrothermal conditions, these components assemble into a mixed-valence cage. Single-crystal X-ray diffraction shows that the cage contains two fused {Mo96} half-shells. The closed cage also contains inward sulfate-bound {S-Mo6} units and continuous windows. The sulfate ligands point toward the inner cavity and support the shell from the inside. In this arrangement, the outer Mo–O surface remains accessible. The cage was further evaluated in TBHP-driven oxidation of hindered phenols. It showed high conversion, high selectivity, and good recyclability. This structure provides a useful example of how internal anion support can be combined with external site accessibility in a giant mixed-valence POM cage.

2 Results and discussion

2.1 Synthesis and formulation of {Mo192}

The {Mo192} cage was obtained as dark-blue lamellar crystals under acidic, reducing, and hydrothermal conditions (Fig. S1). In a typical synthesis, Waugh-type $K_6MnMo_9O_{32}\cdot 6H_2O$ and $Na_2MoO_4\cdot 2H_2O$ were reacted at 130 °C for 72 h in the presence of H_2SO_4 and $N_2H_4\cdot 2HCl$. S Single-crystal X-ray diffraction reveals no Mn or Co sites in the crystallographically resolved {Mo192} framework, while bulk ICP-OES analysis further confirms the absence of Mn and Co in the isolated product. Thus, the Waugh-type {$MnMo_9$} precursor serves as a Mo-containing precursor under the reaction conditions, whereas Mn is not retained in the final cluster framework. Cobalt acetate and L-glutamic acid may act as crystallization aids by helping to establish a suitable reaction and crystallization environment. H_2SO_4 provides both acidity and sulfate anions, while $N_2H_4\cdot 2HCl$ adjusts the reduction degree required to stabilize the mixed-valence framework.

The use of the Waugh-type precursor is important. It supplies a preorganized Mo–O fragment and avoids relying only on the condensation of monomeric molybdate. Under strongly acidic and reducing conditions, direct molybdate condensation can lead to competing products. Control experiments showed that the H_2SO_4 amount and temperature were important for isolating the crystalline product (Table S2). A lower H_2SO_4 amount favored K-{Mo102} [34], whereas temperatures below 120 °C gave amorphous precipitates. These observations indicate that the sulfate-containing acidic medium, the reducing environment, and the hydrothermal temperature all affect the formation of crystalline {Mo192}.

The compound was formulated as $K_6Na_{20}[H_{44}Mo^{VI}_{130}Mo^{V}_{62}O_{548}(H_2O)_{102}(OH)_{44}(SO_4)_{10}]\cdot 238H_2O$. This formulation is supported by single-crystal X-ray diffraction, elemental analysis, redox titration, bond-valence-sum analysis, XPS, solid-state UV–vis spectroscopy, and thermogravimetric analysis (Figs. S10, S11, and S14, Table S4, and Tables S7(a)–S7(c)). The compound is denoted as {Mo192} below.

2.2 Overall structure of {Mo192}

Single-crystal X-ray diffraction reveals that {Mo192} is a fully closed capsule-shaped molybdenum blue cage (Fig. 1). For descriptive purposes, the crystallographically determined framework can be divided into two complementary {Mo96}-type portions that join across the equatorial region to generate the final closed cage with continuous windows. This retrospective structural subdivision is introduced to visualize the overall connectivity and shell closure of the final solid-state framework; it does not indicate the existence of discrete {Mo96} species or establish a stepwise assembly sequence in solution. The outer dimensions are ca. 2.46 × 2.46 × 3.84 nm, and the internal cavity is ca. 2.05 × 2.05 × 3.39 nm according to the crystallographic model (Fig. S7).

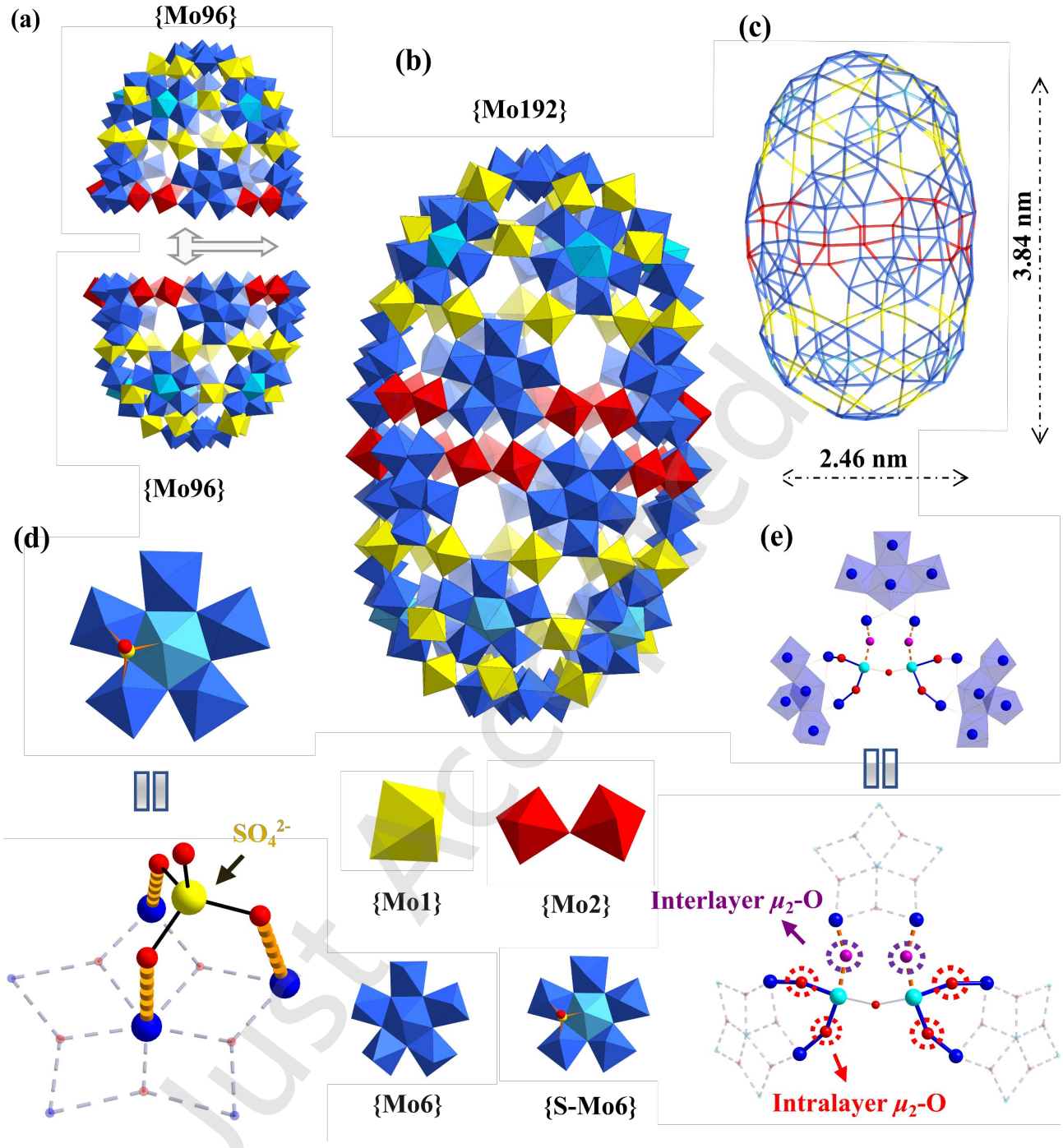

Figure 1 Structure of the fully closed {Mo192} molybdenum blue cage. (a) Two complementary {Mo96}-type structural portions used to illustrate the organization of the final {Mo192} framework. (b) Polyhedral view of the complete {Mo192} cage and the main building units. (c) Wire representation showing the capsule shape and outer dimensions. (d) Inward sulfate-bound {S-Mo6} pentagonal motif. (e) Equatorial {Mo2}-based six-point anchoring motif with intra- and interlayer μ_2-O bridges. Counter cations, lattice water molecules, and hydrogen atoms are omitted for clarity. The colors of the polyhedra are used solely to distinguish the structural building-unit partitions of the {Mo192} framework: {Mo1}, yellow; {Mo2}, red; {Mo6}, blue; and sulfate-bound {S-Mo6}, cyan/blue. These polyhedral colors do not denote elemental identities. In the ball-and-stick and wire representations, elemental identities are indicated separately, with S shown in yellow, Mo shown in blue and O shown in red.

The shell is built from four main types of units: {Mo1}, {Mo2}, pentagonal {Mo6}, and inward sulfate-bound {S-Mo6} units (Fig. 1(b), 1(d), and 1(e); Fig. S3) [17,24,25]. In total, ten {S-Mo6} pentagons and twelve regular {Mo6} pentagons are embedded in the cage. These pentagonal motifs are connected by 40 {Mo1} and 10 {Mo2} units. Together, they form a closed mixed-valence framework with curved pentagonal regions, linker-rich regions, and continuous openings on the shell.

For clarity, the {Mo192} cage can also be described using three larger structural regions (Fig. 2). These are the sulfate-rich curved {S5-Mo35} regions, the equatorial {Mo100} belt, and the polar {Mo11} caps. The {S5-Mo35} regions contain the inward-facing {S-Mo6} units. The {Mo100} belt contains the {Mo2}-based anchoring nodes, and the {Mo11} caps close the

two polar ends of the cage. The {S5-Mo35}, {Mo100}, and {Mo11} regions are defined here as convenient structural domains within the final crystallographic model. Their identification highlights the spatial distribution of sulfate-bound motifs, equatorial linkages, and polar closing units, rather than proposing preformed fragments or directly observed intermediates during self-assembly.

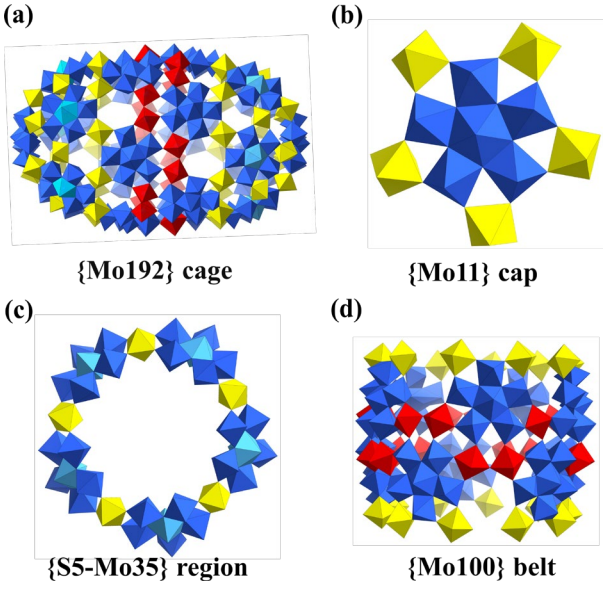

Figure 2 Crystallographic partition of the {Mo192} capsule. (a) Complete {Mo192} cage shown as the structural reference. (b) Polar {Mo11} cap. (c) Sulfate-rich curved {S5-Mo35} region containing inward sulfate-bound {S-Mo6} units. (d) Equatorial {Mo100} belt containing {Mo2}-based anchoring nodes. The highlighted regions represent structural domains defined from the final crystallographic model to visualize the spatial organization and connectivity of the cage; they do not represent discrete precursors, growth fragments, or an experimentally established assembly pathway. Counter cations, lattice water molecules, and hydrogen atoms are omitted for clarity. The polyhedral colors are used solely to visualize the structural partitioning of the {Mo192} framework: {Mo1}, yellow; {Mo2}, red; {Mo6}, blue; and sulfate-bound {S-Mo6}, cyan/blue. These colors identify structural building-unit types rather than chemical elements.

2.3 Inward sulfate coordination and equatorial shell closure

An important structural feature of {Mo192} is the inward coordination of sulfate within the {S-Mo6} units. Sulfate and sulfite ligands are known to act as internal supports in molybdenum blue clusters [14,17,28,29], but their arrangement in {Mo192} is directly connected to the closure of the cage. In each {S-Mo6} unit, sulfate binds to three Mo centers from the inner side of the shell (Fig. 1(d) and Fig. S4). This binding mode distorts the local Mo–O polyhedra and helps generate the curvature required for shell closure. The regular {Mo6} units provide the common pentagonal curvature found in many MB structures, whereas the sulfate-bound {S-Mo6} units introduce additional inward distortion.

The two types of pentagonal units therefore play complementary roles. The regular {Mo6} units provide a familiar curved motif. The sulfate-bound {S-Mo6} units introduce inwardly directed sulfate coordination into curved regions of the shell and are associated with the local bending required by the closed capsule geometry. Because the sulfate ligands point toward the inner cavity, they do not block the outer surface of the cage (Figs. S6 and S8). This inward orientation allows the sulfate ligands to act as internal structural supports while preserving access to external Mo sites for substrates and oxidants.

At the equatorial region, {Mo2} units connect neighbouring {Mo6} units through μ_2-O bridges, giving a six-point anchoring motif (Fig. 1(e)). These connections strengthen the belt where the two curved half-shells meet and help stabilize the closed seam of the capsule. The equatorial belt therefore acts not only as a geometric joint but also as a stabilizing element for the closed capsule. Together with the inward sulfate-bound pentagons, the equatorial {Mo2}-linked belt defines the closed-shell connectivity of the cage.

2.4 Mixed valence and surface accessibility

Redox titration and XPS support a mixed Mo^{VI}/Mo^{V} framework with an overall reduction degree of ca. 32% (Fig. S11 and Tables S7(a)–S7(c)). The crystallographic model and BVS analysis suggest that the Mo^{V} character is concentrated mainly in the {Mo1} units, with possible contributions from the {Mo2} and {Mo6} units. This interpretation is consistent with previous structural studies showing that reduced Mo character is often associated with backbone or bridging units in molybdenum blue frameworks, whereas the pentagonal {Mo6} units are comparatively less reduced [23,29,31]. However, because mixed valence can be delocalized over the cluster and potential crystallographic disorder may affect local BVS values, the BVS results do not provide an unambiguous assignment of the oxidation state of each individual Mo site.

The crystallographic Mo–O bond lengths, oxygen-site BVS values, and charge-balance considerations are consistent with the presence of terminal oxo, hydroxyl, and aqua/protonated oxygen environments in the shell (Figs. S8 and S10 and Table S7(c)). These assignments are based on combined structural and compositional evidence rather than on BVS analysis alone. Thermogravimetric analysis mainly supports the overall dehydration behavior and water content, whereas the detailed oxygen-site assignments are derived primarily from the crystallographic model and are supported by BVS analysis and charge-balance considerations. The cage is therefore not a completely inert oxide surface. Redox-active Mo centers and labile surface ligands coexist in the closed framework. The continuous windows may allow substrates and oxidants to approach the cage surface. Previous studies of porous {Mo132}-type capsules have shown that internal Mo sites and confined water molecules can participate in catalytic transformations [38,40], while guest and ligand exchange through the capsule pores has also been demonstrated [39]. In the present {Mo192} cage, the sulfate ligands are oriented toward the inner cavity, while terminal oxo and aqua/protonated Mo–O environments remain exposed on the outer surface. These external Mo–O environments are therefore accessible to the reaction components. The combination of inward structural support and outward site accessibility is consistent with the efficient TBHP oxidation of sterically hindered phenols.

2.5 Catalytic oxidation of hindered phenols

With the structure established, we evaluated {Mo192} in the oxidation of hindered phenols. 2-tert-Butylphenol was selected as the model substrate, and 2-tert-butyl-*p*-benzoquinone was the target product [41,42,46,48]. This reaction is a useful test because steric hindrance limits access to catalytic sites, while side oxidation can lower selectivity.

The reaction conditions were optimized by screening the solvent, catalyst loading, and temperature (Fig. S13(b) and Table S3). Dichloromethane gave the best balance between conversion and selectivity among the tested solvents. This may be related to the solubility of both substrate and product and to efficient contact with the external Mo sites of the cage. Lower catalyst loading slowed the reaction, while increasing the amount from 3.0 to 5.0 mg gave no clear improvement. A temperature of 70 °C was selected as a practical condition that balanced activity and operational robustness. The optimized conditions were therefore set as follows: {Mo192} (3.0 mg) as the catalyst, TBHP as the oxidant, dichloromethane as the solvent, and 70 °C in a sealed vial.

Under these conditions, 2-tert-butylphenol was converted in 6 h, giving 99% conversion and 99% selectivity (Fig. 3(a) and Table S3). The high selectivity observed for 2-tert-butylphenol may result from the combination of accessible external Mo–O environments and the steric properties of the substrate. The inward-facing sulfate ligands do not directly block the outer Mo sites, which may allow the phenol and TBHP to approach the external surface. At the same time, the bulky tert-butyl group may reduce the probability of further oxidation or oxidative coupling, thereby favoring the formation of the quinone product. This provides a possible explanation for the high quinone selectivity. The observed selectivity may therefore reflect the combined effects of substrate sterics, substrate orientation, electronic properties, and the local Mo–O environment. Control experiments showed much lower activity for {Mo40} [50], $(NH_4)_{10}[H_2W_{12}O_{42}]\cdot xH_2O$ ({W12}), $Na_2MoO_4\cdot 2H_2O$, and the Waugh-type precursor $\{MnMo_9\}$ under the same conditions (Fig. 3(a) and Table S3). The reaction without catalyst or without TBHP was also inefficient (Table S3). All catalytic comparisons were conducted using the same catalyst mass (3.0 mg) under otherwise identical reaction conditions. Because the tested materials differ substantially in molecular weight, nuclearity, composition, and Mo/W content, these experiments should therefore be regarded as mass-matched control experiments rather than strictly metal-normalized activity comparisons. Nevertheless, the results show that the superior performance observed for {Mo192} is not reproduced by the lower-nuclearity molybdate cluster, polytungstate, simple molybdate salt, or Waugh-type precursor under the present conditions. These comparisons support the intact mixed-valence {Mo192} capsule as the principal recoverable catalytic phase associated with the observed high conversion and selectivity.

2.6 Recoverability, stability, and substrate scope

A hot-filtration experiment was performed to examine catalyst leaching. After the solid catalyst was removed at 4 h, the clear filtrate showed only a slight further increase in conversion, whereas the unfiltered reaction continued to 99% conversion (Fig. 3(b) and Fig. S13(a)). ICP-OES analysis showed only trace Mo in the filtrates collected after 4 h hot-filtration, after completion of the standard 6 h reaction, and after the fifth catalytic cycle (Table S8). These results indicate that Mo leaching remains very low throughout the complete reaction and during repeated catalytic use. Together with the hot-filtration experiment and the retained FT-IR and PXRD features after catalysis, the data argue against a dominant contribution from leached Mo species. Very minor solution-phase processes cannot be fully excluded, but the results support {Mo192} as the major recoverable catalytic phase under the present conditions.

The catalyst was reused for five cycles. The conversion decreased from 99% to 89%, while the selectivity remained above 98% (Fig. 3(c) and Fig. S13(c)). The retained selectivity suggests that the main oxidation pathway remains largely unchanged during recycling. FT-IR and PXRD spectra after recycling retained the main framework features of {Mo192} (Figs. S15 and S16). The moderate activity loss may arise from physical loss during recovery or minor surface changes; the post-catalysis FT-IR and PXRD data do not indicate collapse of the main framework.

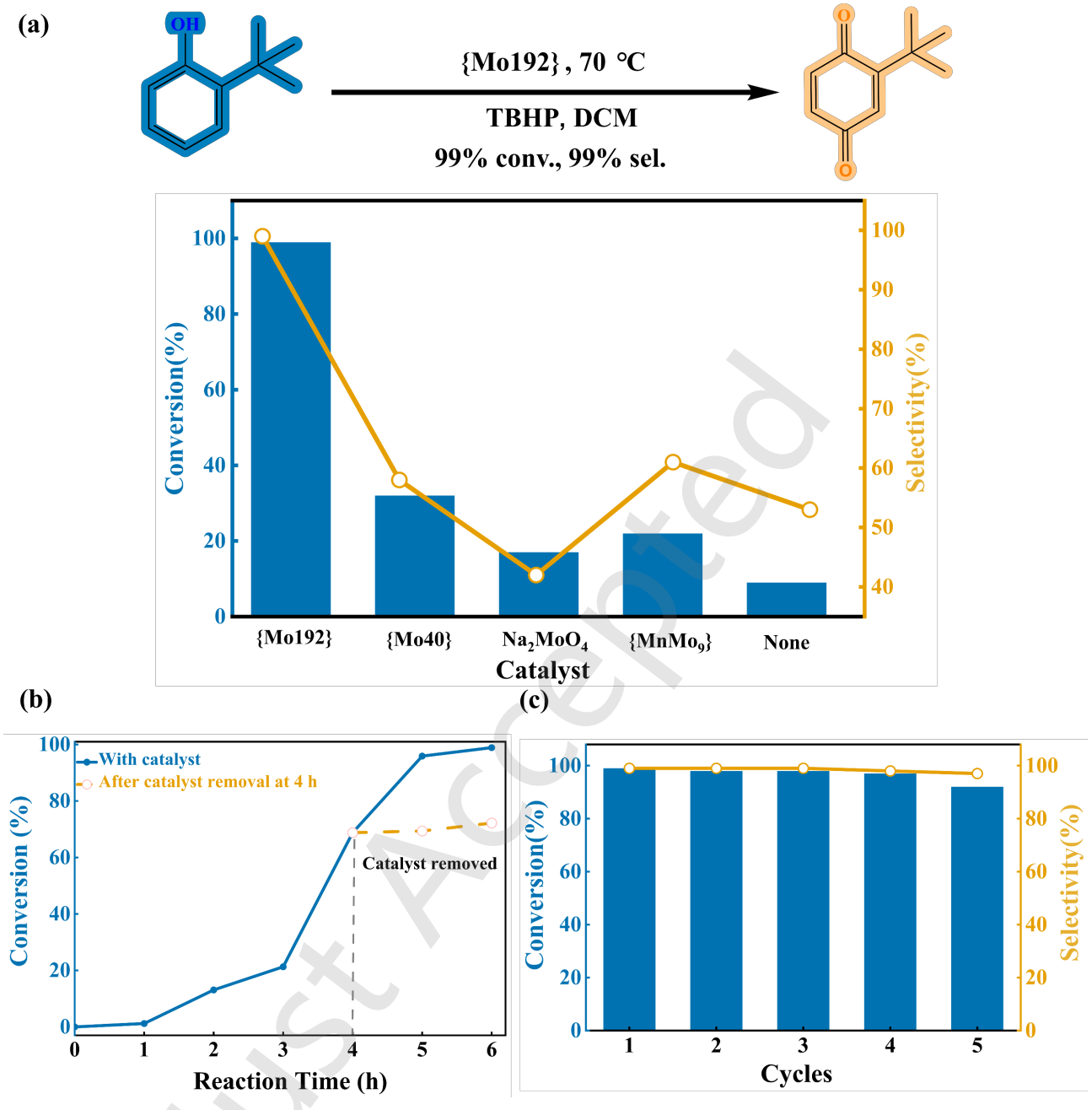

Figure 3 Catalytic performance of {Mo192} in the oxidation of 2-tert-butylphenol. (a) Oxidation of 2-tert-butylphenol to 2-tert-butyl-*p*-benzoquinone and catalyst comparison under the optimized conditions. Blue bars show conversion, and orange lines show selectivity. (b) Hot-filtration test with catalyst removal after 4 h. (c) Recycling of {Mo192} over five runs. Reaction conditions: substrate, 0.10 mmol; TBHP, 1.0 mmol; catalyst, 3.0 mg; dichloromethane, 2.0 mL; 70 °C; sealed vial. For the catalyst comparison in (a), all tested catalysts were used at the same mass loading (3.0 mg); thus, the results represent mass-matched comparisons rather than metal-normalized activity comparisons. Conversion and selectivity were determined by GC using naphthalene as the internal standard.

Several alkyl-substituted phenols were also oxidized under the optimized conditions, giving quinone or quinone-type products with good selectivity in most cases (Fig. 4). These substrates contain methyl or tert-butyl substituents and differ in steric demand and electronic properties. Their conversions varied more than their selectivities. The lower conversion observed for some substrates may result from slower approach to, or less favorable interaction with, the external Mo–O sites. Differences in substrate solubility and substituent effects may also contribute to the observed variation. Thus, steric hindrance may decrease the overall conversion by slowing substrate approach, while simultaneously suppressing some undesired oxidation pathways and preserving selectivity.

The relatively high selectivities observed for the hindered phenols may therefore reflect the suppression of secondary oxidation or oxidative coupling. This effect may be related to the steric environment of the substrates and their interaction with the accessible external Mo–O surface. Taken together, these factors may account for the substrate-dependent

conversion and selectivity observed in Fig. 4. Product assignments were supported by GC–MS and by ^{1}H NMR spectra of the products obtained from the substrate-scope reactions, as shown in Figs. S24–S28. Conversions and selectivities were determined by GC using naphthalene as the internal standard. These results indicate that {Mo192} is a selective and recyclable catalyst for the TBHP oxidation of hindered phenols under the tested conditions.

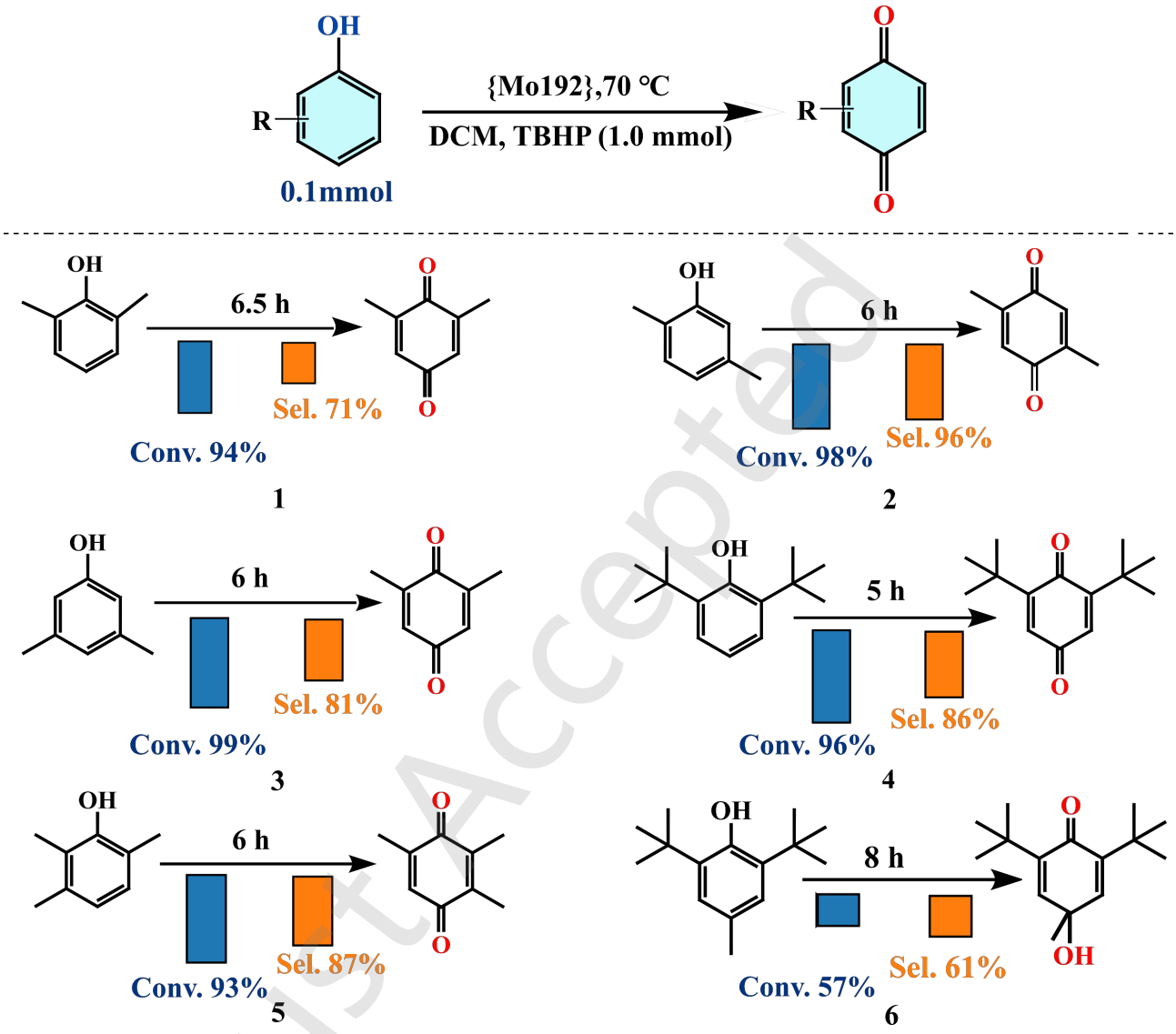

Figure 4 Substrate scope for the TBHP oxidation of alkyl-substituted phenols catalyzed by {Mo192}. Reaction times for individual substrates are indicated in the figure. Unless otherwise noted, reaction conditions were as follows: substrate, 0.10 mmol; TBHP, 1.0 mmol; {Mo192}, 3.0 mg; dichloromethane, 2.0 mL; 70 °C; sealed vial. Conversion and selectivity were determined by GC using naphthalene as the internal standard. Product assignments were supported by GC–MS spectra shown in Figs. S17–S23 and by ^{1}H NMR spectra of representative products shown in Figs. S24–S28.

3 Conclusion

In summary, we synthesized a fully closed capsule-shaped molybdenum blue cage, {Mo192}, through a sulfate-guided fragment/anion co-assembly route. The cage consists of two fused {Mo96} half-shells and contains inward sulfate-bound {S-Mo6} units, equatorial {Mo2}-based anchoring motifs, continuous windows, and a mixed-valence Mo^{VI}/Mo^{V} framework. The sulfate ligands are located on the cavity side of the shell, where they support the curved framework from the inside. The outer Mo–O surface, in contrast, retains accessible terminal oxo and aqua/protonated sites. As a result, {Mo192} combines internal anion support, closed-shell connectivity, and external surface accessibility in one giant POM cage. In oxidation catalysis, {Mo192} promotes the TBHP-driven oxidation of hindered phenols with high conversion, high selectivity, and good recyclability. Hot-filtration, ICP-OES, FT-IR, and PXRD analyses support {Mo192} as the major recoverable catalytic phase under the present conditions. These results show that inward anion coordination is a useful structural tool for accessing fully closed mixed-valence POM cages with retained external functionality. More broadly, the combination of inwardly directed anion coordination and retained external Mo–O accessibility provides a potentially useful structural design principle for developing other closed mixed-valence POM

cages with tunable cavity environments and surface reactivity.

Electronic Supplementary Material: Supplementary material (catalytic details; X-ray crystallographic data; TGA, UV–vis, and PXRD data for {Mo192} before and after catalysis; and additional structural and characterization figures for {Mo192}) is available in the online version of this article at https://doi.org/10.26599/POM.2026.9140158.

Data availability

All data needed to support the conclusions in the paper are presented in the manuscript and the Electronic Supplementary Material. Additional data related to this paper may be requested from the corresponding author upon request.

Acknowledgements

This work is granted by the National Natural Science Foundation of China (Grants 22271075 and 22171071).

Declaration of competing interest

All the contributing author(s) report(s) no conflict of interests in this work.

Author contribution statement

Jialiang Sun: synthesis, catalytic experiments, writing – original draft, and writing – review and editing. Huili Fan and Haojie Xu: synthetic experiments. Pengtao Ma: crystal structure analysis. Chao Zhang, Jingping Wang, and Jingyang Niu: supervision, project administration, discussion of results, and manuscript revision. All authors approved the final version of the manuscript.

Use of AI statement

None.

References

[1] M. T. Pope, A. Müller, Polyoxometalate Chemistry: An Old Field with New Dimensions in Several Disciplines *Angew. Chem. Int. Ed*. **1991**, *30*, 34–48.

[2] D. Long, R. Tsunashima, L. Cronin, Polyoxometalates: Building Blocks for Functional Nanoscale Systems *Angew. Chem. Int. Ed*. **2010**, *49*, 1736–1758.

[3] A. Misra, K. Kozma, C. Streb, M. Nyman, Beyond Charge Balance: Counter-Cations in Polyoxometalate Chemistry *Angew. Chem. Int. Ed*. **2020**, *59*, 596–612.

[4] J.-C. Liu, J.-W. Zhao, C. Streb, Y.-F. Song, Recent advances on high-nuclear polyoxometalate clusters *Coord. Chem. Rev*. **2022**, *471*, 214734.

[5] I. A. Weinstock, R. E. Schreiber, R. Neumann, Dioxygen in Polyoxometalate Mediated Reactions *Chem. Rev*. **2018**, *118*, 2680–2717.

[6] O. A. Kholdeeva, O. V. Zalomaeva, Recent advances in transition-metal-catalyzed selective oxidation of substituted phenols and methoxyarenes with environmentally benign oxidants *Coord. Chem. Rev*. **2016**, *306*, 302–330.

[7] N. Li, J. Liu, B. Dong, Y. Lan, Polyoxometalate-Based Compounds for Photo- and Electrocatalytic Applications *Angew. Chem. Int. Ed*. **2020**, *59*, 20779–20793.

[8] Z. Li, Y. Zeng, Y. Dong, H. Lv, G.-Y. Yang, Metal/H^+ sites modulation in the decatungstate+Pd/C catalytic system for photocatalytic generation of furfuryl ethyl ether *Chin. J. Catal*. **2025**, *75*, 137–146.

[9] M. Ren, T. Liu, Y. Dong, Z. Li, J. Yang, Z. Diao, H. Lv, G.-Y. Yang, Near-unity photocatalytic dehydrocoupling of thiophenols into disulfides and hydrogen using coupled CdS Nanorods and Ni-containing polyoxometalate *Chin. J. Catal*. **2024**, *61*, 312–321.

[10] J. Yang, Y. Liu, Y. Qin, Z. Diao, Y. Dong, H. Lv, Controllable photooxidation of 1-phenylethanol integrated with hydrogen evolution by a polyoxometalate/$ZnIn_2S_4$/WO_3 catalytic system *Nano Res*. **2025**, *18*, 94907303.

[11] M. Chi, J. Wei, Y. Wen, Z. Zhao, X. Liu, H. Su, J. Ning, G. Yang, H. Lv, A Small Structural Change Makes a Big Difference: Synthesis of a Bowl-Like Polyoxometalate-Encapsulated $\{Ag_7\}^{5+}$ Cluster and Its Structural Derivatives *Angew. Chem. Int. Ed*. **2026**, e5283794.

[12] Y. Feng, M. Zhao, J. Yang, Z. Wang, P. Bai, Y. Liu, H. Lv, G. Yang, Wearing Gigantic Silver Armor on Transition-Metal-Containing Polyoxometalates: Formation of Supertetrahedral Intercluster Compounds *Angew. Chem. Int. Ed*. **2025**, *64*, e202505511.

[13] Y. Zhi, M. Zhao, Y. Li, Y. Feng, Z. Wen, H. Lv, G.-Y. Yang, Solvent-induced synthesis of structurally new $\{PW_9O_{34}\}$-sandwiched silver alkynyl interclusters *Chin. Chem. Lett*. **2026**, 112987.

[14] A. Müller, P. Gouzerh, From linking of metal-oxide building blocks in a dynamic library to giant clusters with unique properties and towards adaptive chemistry *Chem. Soc. Rev*. **2012**, 41, 7431.

[15] E. Al-Sayed, A. Rompel, "Lanthanides Singing the Blues: Their Fascinating Role in the Assembly of Gigantic Molybdenum Blue Wheels" ACS Nanosci. Au 2022, 2, 179–197.

[16] Long, D.-L.; Cronin, L. Advances in Gigantic Polyoxomolybdate Chemistry. *Adv. Inorg. Chem*. **2021**, *78*, 227–267.

[17] Y. Kuang, Z. Mei, J. Lin, C. Zeng, L. Dong, S. Liang, J. Shi, L. Jin, S. Li, J. Liu, Y. Lan, Lacunary Evolution of Molybdenum Blue Clusters for Efficient and Sustainable Photocatalytic Chemodivergent C─C Coupling Reactions *Angew. Chem. Int. Ed.* **2026**, *65*, e1160992.

[18] A. Müller, E. Krickemeyer, J. Meyer, H. Bögge, F. Peters, W. Plass, E. Diemann, S. Dillinger, F. Nonnenbruch, M. Randerath, C. Menke, $[Mo_{154}(NO)_{14}O_{420}(OH)_{28}(H_2O)_{70}]^{(25\pm5)-}$: A Water-Soluble Big Wheel with More than 700 Atoms and a Relative Molecular Mass of About 24000 *Angew. Chem. Int. Ed.* **1995**, *34*, 2122–2124.

[19] A. Müller, S. Q. N. Shah, H. Bögge, M. Schmidtmann, Molecular growth from a Mo_{176} to a Mo_{248} cluster *Nature* **1999**, *397*, 48–50.

[20] A. Müller, E. Beckmann, H. Bögge, M. Schmidtmann, A. Dress, Inorganic Chemistry Goes Protein Size: A Mo_{368} Nano-Hedgehog Initiating Nanochemistry by Symmetry Breaking *Angew. Chem. Int. Ed.* **2002**, *41*, 1162–1167.

[21] H. N. Miras, C. J. Richmond, D.-L. Long, L. Cronin, Solution-Phase Monitoring of the Structural Evolution of a Molybdenum Blue Nanoring *J. Am. Chem. Soc.* **2012**, *134*, 3816–3824.

[22] H. N. Miras, G. J. T. Cooper, D.-L. Long, H. Bögge, A. Müller, C. Streb, L. Cronin, Unveiling the Transient Template in the Self-Assembly of a Molecular Oxide Nanowheel *Science* **2010**, *327*, 72–74.

[23] M. Cheng, D. Zhang, Y. Liu, Z. Chen, Y. Ma, R. Tang, K. Wang, H. Wang, D.-L. Long, L. Cronin, W. Xuan, Breaking the Boundary of Gigantic Molybdenum Blue Clusters: From Half-Closed $\{Mo_{85}\}$ to $\{Mo_{172}\}$ Dimer *CCS Chem*. **2025**, 1–9.

[24] M. Cheng, Y. Li, R. Tang, Y. Ma, D.-L. Long, L. Cronin, W. Xuan, Organophosphonate Ligation Approach for the Controlled Assembly of Gigantic Polyoxometalate Clusters *J. Am. Chem. Soc*. **2026**, *148*, 12890–12897.

[25] M. Wang, M.-Z. Cai, H.-J. Xu, Y.-F. Zhang, J.-Y. Pang, C. Zhang, P.-T. Ma, J.-P. Wang, J.-Y. Niu, Assembly of a Pebble-Type Giant Polyoxometalate Cage $\{Mo_{108}\}$ for Proton Conduction *Inorg. Chem.* **2025**, *64*, 16470–16477.

[26] A. Müller, E. Krickemeyer, H. Bögge, M. Schmidtmann, F. Peters, Organizational Forms of Matter: An Inorganic Super Fullerene and Keplerate Based on Molybdenum Oxide *Angew. Chem. Int. Ed.* **1998**, *37*, 3359–3363.

[27] J. Liu, N. Jiang, J. Lin, Z. Mei, L. Dong, Y. Kuang, J. Liu, S. Yao, S. Li, Y. Lan, Structural Evolution of Giant Polyoxometalate: From 'Keplerate' to 'Lantern' Type Mo_{132} for Improved Oxidation Catalysis *Angew. Chem. Int. Ed.* **2023**, *62* e202304728.

[28] J.-M. Lin, Z.-B. Mei, C. Guo, J.-R. Li, Y. Kuang, J.-W. Shi, J.-J. Liu, X. Li, S.-L. Li, J. Liu, Y.-Q. Lan, Synthesis of Isotypic Giant Polymolybdate Cages for Efficient Photocatalytic C–C Coupling Reactions *J. Am. Chem. Soc.* **2024**, *146*, 22797–22806.

[29] V. Lakhanpal, M. Guillén-Soler, L. Vilà-Nadal, D.-L. Long, L. Cronin,

Compression of Molybdenum Blue Polyoxometalate Cluster Rings *J. Am. Chem. Soc.* **2025**, *147*, 10579–10586.

[30] W. Xuan, R. Pow, D. Long, L. Cronin, Exploring the Molecular Growth of Two Gigantic Half-Closed Polyoxometalate Clusters {Mo_{180}} and {$Mo_{130}Ce_6$} *Angew. Chem. Int. Ed*. **2017**, *56*, 9727–9731.

[31] X.-X. Li, C.-H. Li, M.-J. Hou, B. Zhu, W.-C. Chen, C.-Y. Sun, Y. Yuan, W. Guan, C. Qin, K.-Z. Shao, X.-L. Wang, Z.-M. Su, Ce-Mediated Molecular Tailoring on Gigantic Polyoxometalate {Mo_{132}} into Half-Closed {$Ce_{11}Mo_{96}$} for High Proton Conduction. *Nat. Commun.* **2023**, *14*, 5025.

[32] D. Zhang, R. Tang, Y. Ma, Q. Zhao, Q. Zheng, Y. Wei, D.-L. Long, L. Cronin, W. Xuan, Dimensional Evolution from a Giant Molybdenum-Red Cage-like {Mo_{200}} to 1D Chains Enabling Ultrahigh Proton Conduction *J. Am. Chem. Soc*. **2026**, *148*, 27603–27612.

[33] H.-M. Zeng, M. Cheng, W. Xuan, Y. Wei, Assembly of the Skirt-Like Giant Molybdenum Blue Cluster {Mo_{158}} from Dimerization of {Mo_{79}} Featuring an Octameric Skeleton *Inorg. Chem*. **2025**, *64*, 67–72.

[34] M. T.-K. Ng, N. L. Bell, D.-L. Long, L. Cronin, Facile and Reproducible Electrochemical Synthesis of the Giant Polyoxomolybdates *J. Am. Chem. Soc.* **2021**, *143*, 20059–20063.

[35] E. Garrido Ribó, N. L. Bell, W. Xuan, J. Luo, D.-L. Long, T. Liu, L. Cronin, Synthesis, Assembly, and Sizing of Neutral, Lanthanide Substituted Molybdenum Blue Wheels {Mo_{90} Ln_{10}} *J. Am. Chem. Soc.* **2020**, *142*, 17508–17514.

[36] J. Lin, N. Li, S. Yang, M. Jia, J. Liu, X.-M. Li, L. An, Q. Tian, L.-Z. Dong, Y.-Q. Lan, Self-Assembly of Giant Mo240 Hollow Opening Dodecahedra *J. Am. Chem. Soc.* **2020**, *142*, 13982–13988.

[37] W. Liu, G. Yu, M. Zhang, R. Li, L. Dong, H. Zhao, Y. Chen, Z. Xin, S. Li, Y. Lan, Investigation of the Enhanced Lithium Battery Storage in a Polyoxometalate Model: From Solid Spheres to Hollow Balls *Small Methods* **2018**, *2*, 1800154.

[38] S. Kopilevich, A. Gil, M. Garcia-Ratés, J. Bonet-Ávalos, C. Bo, A. Müller, I. A. Weinstock, Catalysis in a Porous Molecular Capsule: Activation by Regulated Access to Sixty Metal Centers Spanning a Truncated Icosahedron *J. Am. Chem. Soc*. **2012**, *134*, 13082–13088.

[39] O. Petina, D. Rehder, E. T. K. Haupt, A. Grego, I. A. Weinstock, A. Merca, H. Bögge, J. Szakács, A. Müller, Guests on Different Internal Capsule Sites Exchange with Each Other and with the Outside *Angew. Chem. Int. Ed*. **2011**, *50*, 410–414.

[40] N. A. G. Bandeira, S. Garai, A. Müller, C. Bo, The mechanism of CO_2 hydration: a porous metal oxide nanocapsule catalyst can mimic the biological carbonic anhydrase role *Chem. Commun*. **2015**, *51*, 15596–15599.

[41] S. Chang, Y. Chen, H. An, Q. Zhu, H. Luo, T. Xu, Highly Efficient Synthesis of *p* -Benzoquinones Catalyzed by Robust Two-Dimensional POM-Based Coordination Polymers *ACS Appl. Mater. Interfaces* **2021**, *13*, 21261–21271.

[42] Y. Lin, B. Li, Z. Feng, Y. A. Kim, M. Endo, D. S. Su, Efficient Metal-Free Catalytic Reaction Pathway for Selective Oxidation of Substituted Phenols *ACS Catal.* **2015**, *5*, 5921–5926.

[43] H. An, Y. Wei, Q. Zhu, J. Fu, T. Xu, Polyoxovanadate-Based Metal–Organic Frameworks with Dual Active Sites for the Synthesis of *p*-Benzoquinones *Inorg. Chem.* **2024**, *63*, 11113–11124.

[44] Y. Gu, Q. Li, D. Zang, Y. Huang, H. Yu, Y. Wei, Light-Induced Efficient Hydroxylation of Benzene to Phenol by Quinolinium and Polyoxovanadate-Based Supramolecular Catalysts *Angew. Chem. Int. Ed*. **2021**, *60*, 13310–13316.

[45] K. D. A. Dias, M. V. P. Pereira Junior, L. H. Andrade, Benzoic acid resin (BAR): a heterogeneous redox organocatalyst for continuous flow synthesis of benzoquinones from *β*-O-4 lignin models *Green Chem*. **2021**, *23*, 2308–2316.

[46] X. Bai, M. Zhu, Y. Liu, S. Wang, A. Zhang, C. Sun, Y. Lu, S. Liu, Polyoxometalate-based metal-organic complexes with dual-site synergy for catalytic synthesis of *p*-benzoquinone *Mater. Today Chem.* **2025**, *48*, 102929.

[47] S. Chang, H. An, Y. Chen, Y. Hou, J. Zhang, Q. Zhu, Multiunit Catalysts with Synergistic Reactivity: Three-Dimensional Polyoxometalate-Based Coordination Polymers for Highly Efficient Synthesis of Functionalized *p*-Benzoquinones *ACS Appl. Mater. Interfaces* **2019**, *11*, 37908–37919.

[48] Z. An, X. Li, Z. Zhang, X. Wang, Capped Polyoxometalate-Based Metal–Organic Complex with Mixed-Valence Cu^{I}/Cu^{II} for Synergistic Catalytic Synthesis of *p*-Benzoquinone *Inorg. Chem*. **2024**, *63*, 19956–19963.

[49] J. L. T. Waugh, D. P. Shoemaker, L. Pauling, On the structure of the heteropoly anion in ammonium 9-molybdomanganate, $(NH_4)_6MnMo_9O_{32}.8H_2O$ *Acta Crystallogr.* **1954**, *7*, 438–441.

[50] A. Müller, C. Kuhlmann, H. Bögge, M. Schmidtmann, M. Baumann, E. Krickemeyer, $Mo^{V}_2O_4^{2+}$ Directs the Formation and Subsequent Linking of Potential Building Blocks under Different Boundary Conditions: A Related Set of Novel Cyclic Polyoxomolybdates *Eur. J. Inorg. Chem.* **2001**, *2001*, 2271–2277.

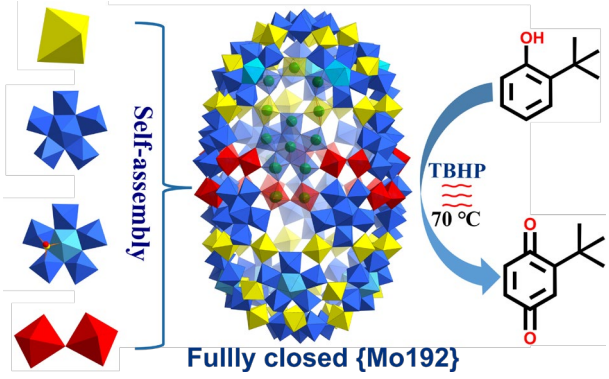

Sulfate-guided assembly affords a fully closed capsule-shaped {Mo192} molybdenum blue cage with inward-facing sulfate ligands and accessible external Mo–O environments. The {Mo192} cage shows high conversion and selectivity in the TBHP-mediated oxidation of hindered phenols to *p*-benzoquinones.